EUROPEAN ORGANISATION FOR NUCLEAR RESEARCH

CERN-PPE/91-48
14 March 1991

A Study of Heavy Flavour Production using Muons in Hadronic Z^0 Decays

The OPAL Collaboration

Abstract

Using muon candidates in 133,000 hadronic decays of the Z^0, recorded by the OPAL detector at LEP, we have measured the fraction of events containing semi-leptonic decays of b flavoured hadrons. An analysis based on fitting the shape of the momentum and transverse momentum distributions of the muon candidates gave the result: $(\Gamma(Z^0 \to b\bar{b})/\Gamma(Z^0 \to \text{hadrons})) \times \text{Br}(b \to \mu) = 0.0226 \pm 0.0007 \pm 0.0013$, and also yielded: $(\Gamma(Z^0 \to c\bar{c})/\Gamma(Z^0 \to \text{hadrons})) \times \text{Br}(c \to \mu) = 0.0176 \pm 0.0025 \pm 0.0042$. Using the charge of the muon and the angle of the event thrust axis with respect to the electron beam, in a b-enriched event sample, we measured the forward-backward asymmetry for $Z^0 \to b\bar{b}$ decays. Without correction for $B^0\bar{B}^0$ mixing, the asymmetry was found to be $A_b^{FB} = 0.072 \pm 0.042 \pm 0.010$.

Submitted to Physics Letters B

The OPAL Collaboration

M.Z. Akrawy[13], G. Alexander[23], J. Allison[16], P.P. Allport[5], K.J. Anderson[9], J.C. Armitage[6], P. Ashton[16], A. Astbury[a], D. Axen[b], G. Azuelos[18,c], J.T.M. Baines[16], A.H. Ball[17], J. Banks[16], G.J. Barker[13], R.J. Barlow[16], J.R. Batley[5], G. Beaudoin[18], A. Beck[23], J. Becker[10], T. Behnke[8], K.W. Bell[20], G. Bella[23], S. Bethke[11], O. Biebel[3], U. Binder[10], I.J. Bloodworth[1], P. Bock[11], S. Bougerolle[b], B.B. Brabson[12], H. Breuker[8], R.M. Brown[20], R. Brun[8], A. Buijs[8], H.J. Burckhart[8], P. Capiluppi[2], R.K. Carnegie[6], A.A. Carter[13], J.R. Carter[5], C.Y. Chang[17], D.G. Charlton[8], J.T.M. Chrin[16], P.E.L. Clarke[25], I. Cohen[23], W.J. Collins[5], J.E. Conboy[15], M. Cooper[22], M. Couch[1], M. Coupland[14], M. Cuffiani[2], S. Dado[22], G.M. Dallavalle[2], S. De Jong[8], P. Debu[21], M.M. Deninno[2], A. Dieckmann[11], M. Dittmar[4], M.S. Dixit[7], E. Duchovni[26], I.P. Duerdoth[16], D.J.P. Dumas[6], P.A. Elcombe[5], P.G. Estabrooks[6], E. Etzion[23], F. Fabbri[2], P. Farthouat[21], M. Fincke-Keeler[a], H.M. Fischer[3], D.G. Fong[17], C. Fukunaga[24], A. Gaidot[21], O. Ganel[26], J.W. Gary[11], J. Gascon[18], N.I. Geddes[20], C. Geich-Gimbel[3], S.W. Gensler[9], F.X. Gentit[21], G. Giacomelli[2], V. Gibson[5], W.R. Gibson[13], J.D. Gillies[20], J. Goldberg[22], M.J. Goodrick[5], W. Gorn[4], E. Gross[26], H. Hagedorn[10], J. Hagemann[8], G.G. Hanson[12], M. Hansroul[8], C.K. Hargrove[7], I. Harrus[22], J. Hart[5], P.M. Hattersley[1], M. Hauschild[8], C.M. Hawkes[8], E. Heflin[4], R.J. Hemingway[6], R.D. Heuer[8], J.C. Hill[5], S.J. Hillier[1], D.A. Hinshaw[18], C. Ho[4], J.D. Hobbs[9], P.R. Hobson[25], D. Hochman[26], B. Holl[8], R.J. Homer[1], S.R. Hou[17], C.P. Howarth[15], R.E. Hughes-Jones[16], R. Humbert[10], P. Igo-Kemenes[11], H. Ihssen[11], D.C. Imrie[25], L. Janissen[6], A. Jawahery[17], P.W. Jeffreys[20], H. Jeremie[18], M. Jimack[8], M. Jobes[1], R.W.L. Jones[13], P. Jovanovic[1], D. Karlen[6], K. Kawagoe[24], T. Kawamoto[24], R.K. Keeler[a], R.G. Kellogg[17], B.W. Kennedy[15], C. Kleinwort[8], D.E. Klem[19], G. Knop[3], T. Kobayashi[24], T.P. Kokott[3], L. Köpke[8], R. Kowalewski[6], H. Kreutzmann[3], J. von Krogh[11], J. Kroll[9], M. Kuwano[24], P. Kyberd[13], G.D. Lafferty[16], F. Lamarche[18], W.J. Larson[4], J.G. Layter[4], P. Le Du[21], P. Leblanc[18], A.M. Lee[17], M.H. Lehto[15], D. Lellouch[8], P. Lennert[11], C. Leroy[18], L. Lessard[18], S. Levegrün[3], L. Levinson[26], S.L. Lloyd[13], F.K. Loebinger[16], J.M. Lorah[17], B. Lorazo[18], M.J. Losty[7], X.C. Lou[12], J. Ludwig[10], M. Mannelli[8], S. Marcellini[2], G. Maringer[3], A.J. Martin[13], J.P. Martin[18], T. Mashimo[24], P. Mättig[3], U. Maur[3], T.J. McMahon[1], J.R. McNutt[25], F. Meijers[8], D. Menszner[11], F.S. Merritt[9], H. Mes[7], A. Michelini[8], R.P. Middleton[20], G. Mikenberg[26], J. Mildenberger[6], D.J. Miller[15], C. Milstene[23], M. Minowa[24], W. Mohr[10], C. Moisan[18], A. Montanari[2], T. Mori[24], M.W. Moss[16], P.G. Murphy[16], W.J. Murray[5], B. Nellen[3], H.H. Nguyen[9], M. Nozaki[24], S.W. O'Neale[8,d], B.P. O'Neill[4], F.G. Oakham[7], F. Odorici[2], M. Ogg[6], H.O. Ogren[12], H. Oh[4], C.J. Oram[e], M.J. Oreglia[9], S. Orito[24], J.P. Pansart[21], P. Paschievici[26], G.N. Patrick[20], S.J. Pawley[16], P. Pfister[10], J.E. Pilcher[9], J.L. Pinfold[26], D.E. Plane[8], P. Poffenberger[a], B. Poli[2], A. Pouladdej[6], E. Prebys[8], T.W. Pritchard[13], H. Przysiezniak[18], G. Quast[8], M.W. Redmond[9], D.L. Rees[1], M. Regimbald[18], K. Riles[4], C.M. Roach[5], S.A. Robins[13], A. Rollnik[3], J.M. Roney[9], S. Rossberg[10], A.M. Rossi[2,f], P. Routenburg[6], K. Runge[10], O. Runolfsson[8], D.R. Rust[12], S. Sanghera[6], M. Sasaki[24], A.D. Schaile[10], O. Schaile[10], W. Schappert[6], P. Scharff-Hansen[8], P. Schenk[a], H. von der Schmitt[11], S. Schreiber[3], J. Schwarz[10], M. Settles[12], B.C. Shen[4], P. Sherwood[15], R. Shypit[b], A. Simon[3], P. Singh[13], G.P. Siroli[2], A. Skuja[17], A.M. Smith[8], T.J. Smith[8], G.A. Snow[17], R. Sobie[g], R.W. Springer[17], M. Sproston[20], K. Stephens[16], H.E. Stier[10], R. Stroehmer[11], D. Strom[9], H. Takeda[24], T. Takeshita[24], P. Taras[18], S. Tarem[26], N.J. Thackray[1], T. Tsukamoto[24], M.F. Turner[5], G. Tysarczyk-Niemeyer[11], D. Van den plas[18], R. Van Kooten[8], G.J. VanDalen[4], G. Vasseur[21], C.J. Virtue[19], A. Wagner[11], C. Wahl[10], J.P. Walker[1], C.P. Ward[5], D.R. Ward[5], P.M. Watkins[1], A.T. Watson[1], N.K. Watson[1], M. Weber[11], S. Weisz[8], P.S. Wells[8], N. Wermes[11], M. Weymann[8], G.W. Wilson[21], J.A. Wilson[1], I. Wingerter[8], V-H. Winterer[10], N.C. Wood[15], S. Wotton[8], T.R. Wyatt[16], R. Yaari[26], Y. Yang[4,h], G. Yekutieli[26], T. Yoshida[24], I. Zacharov[8], W. Zeuner[8], G.T. Zorn[17].

[1]School of Physics and Space Research, University of Birmingham, Birmingham, B15 2TT, UK
[2]Dipartimento di Fisica dell' Università di Bologna and INFN, Bologna, 40126, Italy
[3]Physikalisches Institut, Universität Bonn, D-5300 Bonn 1, FRG
[4]Department of Physics, University of California, Riverside, CA 92521 USA
[5]Cavendish Laboratory, Cambridge, CB3 0HE, UK
[6]Carleton University, Dept of Physics, Colonel By Drive, Ottawa, Ontario K1S 5B6, Canada
[7]Centre for Research in Particle Physics, Carleton University, Ottawa, Ontario K1S 5B6, Canada
[8]CERN, European Organisation for Particle Physics, 1211 Geneva 23, Switzerland
[9]Enrico Fermi Institute and Department of Physics, University of Chicago, Chicago Illinois 60637, USA
[10]Fakultät für Physik, Albert Ludwigs Universität, D-7800 Freiburg, FRG
[11]Physikalisches Institut, Universität Heidelberg, Heidelberg, FRG
[12]Indiana University, Dept of Physics, Swain Hall West 117, Bloomington, Indiana 47405, USA
[13]Queen Mary and Westfield College, University of London, London, E1 4NS, UK
[14]Birkbeck College, London, WC1E 7HV, UK
[15]University College London, London, WC1E 6BT, UK
[16]Department of Physics, Schuster Laboratory, The University, Manchester, M13 9PL, UK
[17]Department of Physics and Astronomy, University of Maryland, College Park, Maryland 20742, USA
[18]Laboratoire de Physique Nucléaire, Université de Montréal, Montréal, Quebec, H3C 3J7, Canada
[19]National Research Council of Canada, Herzberg Institute of Astrophysics, Ottawa, Ontario K1A 0R6, Canada
[20]Rutherford Appleton Laboratory, Chilton, Didcot, Oxfordshire, OX11 0QX, UK
[21]DPhPE, CEN Saclay, F-91191 Gif-sur-Yvette, France
[22]Department of Physics, Technion-Israel Institute of Technology, Haifa 32000, Israel
[23]Department of Physics and Astronomy, Tel Aviv University, Tel Aviv 69978, Israel
[24]International Centre for Elementary Particle Physics and Dept of Physics, University of Tokyo, Tokyo 113, and Kobe University, Kobe 657, Japan
[25]Brunel University, Uxbridge, Middlesex, UB8 3PH UK
[26]Nuclear Physics Department, Weizmann Institute of Science, Rehovot, 76100, Israel
[§]University of British Columbia, Dept of Physics, 6224 Agriculture Road, Vancouver BC V6T 2A6, Canada
[§§]University of Victoria, Dept of Physics, P O Box 1700, Victoria BC V8W 2Y2, Canada

[a]Univ of Victoria, Victoria, Canada
[b]Univ of British Columbia, Vancouver, Canada
[c]and TRIUMF, Vancouver, Canada
[d]On leave from Birmingham University
[e]Univ of Victoria, and TRIUMF, Canada
[f]Present address: Dipartimento di Fisica, Università della Calabria and INFN, 87036 Rende, Italy
[g]Univ of British Columbia and IPP, Canada
[h]On leave from Research Institute for Computer Peripherals, Hangzhou, China

1 Introduction

The data from LEP and SLC have permitted precise measurements of the Z^0 total width, as well as the partial widths into lepton pairs and into hadrons. With these results, the number of light neutrino generations and the Z^0 coupling to leptons have been established [1]. Determination of the Z^0 coupling to quarks and the forward-backward charge asymmetry for $Z^0 \to q\bar{q}$ provide additional tests of the predictions of the Standard Model. A precision measurement of the partial width for $Z^0 \to b\bar{b}$ has been proposed as an important test of radiative corrections in the electroweak model [2], while the forward-backward charge asymmetry is sensitive to the value of the weak mixing angle [3].

In this article, we describe a measurement of the partial width and the forward-backward charge asymmetry for the process $Z^0 \to b\bar{b}$, the partial width for the process $Z^0 \to c\bar{c}$, and the fragmentation parameters of the b and c quarks. Several measurements of these quantities have recently been reported [4,5]. The following study was based on an analysis of multihadronic events containing muons, in data recorded with the OPAL detector at LEP. The data correspond to approximately 133,000 hadronic Z^0 decays and an integrated luminosity of 6.4 pb^{-1} at and around the Z^0 peak. The processes $Z^0 \to b\bar{b}$ and $Z^0 \to c\bar{c}$ were distinguished from $Z^0 \to u\bar{u}, d\bar{d}, s\bar{s}$ events using the muons from semi-leptonic weak decays. Muons were identified via their ability to penetrate material.

In hadronic decays of the Z^0, the penetrating tracks originate from several sources:

(a) $Z^0 \to b\bar{b}$, followed by[1] $b \to \mu^-$.

(b) The cascade reaction, $Z^0 \to b\bar{b}$, followed by $b \to c \to \mu^+$, or $b \to \bar{c} \to \mu^-$ where the $\bar{c}$ quark originates from the virtual W produced in the b quark decay.

(c) $Z^0 \to b\bar{b}$, followed by $b \to \tau^- \to \mu^-$.

(d) $Z^0 \to c\bar{c}$, followed by $c \to \mu^+$.

(e) Hadronic contamination, which comprises sail-through (hadrons which do not interact in the material), punch-through (hadrons whose interaction products penetrate the material), and muons from decays of kaons and pions.

The categories (a) to (d) are collectively referred to as prompt muons.

The hard fragmentation of the b quark and its large mass result in the muons from the decay of b flavoured hadrons having high momentum, p, and transverse momentum, p_T, relative to the direction of the parent hadron. The charm and cascade decays yield considerably softer distributions in both variables, which allows b and c decays to be separated on a statistical basis by applying kinematic cuts, or by fitting.

[1]Throughout this paper, reference to a b or c quark decay is assumed to imply the charge conjugate process for $\bar{b}$ and $\bar{c}$.

2 The OPAL Detector

The OPAL detector has been described in detail in a recent publication [6], and we restrict ourselves to an overview of the main components. Tracking of charged particles is performed by the jet chamber, a large volume drift chamber, 4m long and 3.7m in diameter, divided into 24 azimuthal[2] sectors with 159 layers of wires. The jet chamber, a vertex detector, and chambers measuring the z coordinate of tracks as they leave the jet chamber, are positioned inside a solenoidal coil, which provides a uniform magnetic field of 0.435 T. This coil is surrounded by a time-of-flight counter array and a lead glass electromagnetic calorimeter with a presampler. Outside this calorimeter is the instrumented return yoke of the magnet, forming the hadron calorimeter, and beyond this are the outer muon detectors.

The hadron calorimeter, the muon barrel and muon endcap together form the muon identification system, which covers polar angles in the range $|\cos\theta| < 0.98$. Hadrons are filtered out by the material in the coil, the lead glass calorimeter and the iron return yoke of the magnet. Together these components provide between 6 and 9 interaction lengths, depending on the orientation of the tracks. The barrel region of the muon chambers, covering the region $|\cos\theta| < 0.68$, consists of four layers of planar drift chambers, providing measurements in the (r, ϕ) plane. The endcap region $0.60 < |\cos\theta| < 0.98$ is covered by four layers of limited streamer tubes, each layer measuring in the (x,z) and the (y,z) planes. The hadron calorimeter, which consists of 9 layers (8 layers in the endcap) of streamer tubes interleaved with the iron slabs of the magnet return yoke, is read out via 4 mm wide strips and projective towers formed from 50×50 cm^2 pads. These strips and pads provide measurements in the (r, ϕ) plane and the z direction, respectively. For most of the angular coverage of the detector ($|\cos\theta| < 0.69$) a penetrating track is measured both in the hadron calorimeter and in the muon chambers. The minimum momentum required for a prompt muon to penetrate to the muon chambers, irrespective of polar angle, is 3 GeV/c.

3 Selection and Simulation of Hadronic Events

The trigger and selection criteria for hadronic events have been described in previous publications [7]. In addition, for this analysis, the jet chamber, hadron calorimeter, and the barrel and endcap muon chambers were required to be fully operational. Each event was also required to contain at least seven charged tracks originating from the event vertex, with a distance of closest approach in the direction perpendicular to the beam axis of less than 2 cm and in the direction along the beam of less than 40 cm. The track multiplicity cut reduced the residual contamination from $e^+e^- \to \tau^+\tau^-$ to less than 0.1%.

Any event containing a track with a measured momentum exceeding 45 GeV/c was rejected because of the possible bias to jet and thrust axes caused by such tracks. An additional 0.5% of events were eliminated by this cut. A total of 133,310 events satisfied all the above requirements. The efficiency of these criteria for selecting multihadronic Z^0 decays was (97.0 ± 1.0)%.

The Lund parton shower Monte Carlo JETSET 7.2 [8], was used to simulate multihadronic decays of the Z^0. The Monte Carlo input parameters were chosen to give the best simulation of the observed global event shape distributions [9]. All b quarks were assumed to decay to c

[2]The coordinate system is defined with positive z along the outgoing e^- beam direction, θ and ϕ being the polar and azimuthal angles.

quarks, with the accompanying virtual W coupling to a $\bar{c}$ quark 15% of the time. The product branching ratio $b \to \tau \to \mu$ was taken to be 0.9% [10,11]. Heavy quarks were fragmented according to the Peterson scheme [12], where the shape of the primordial fragmentation function for flavour q depends upon the single parameter ϵ_q. This parameter determines the physical quantity $\langle x_E \rangle_q$, where $x_E = 2 \times E_{Hadron}/\sqrt{s}$, and E_{Hadron} is the energy of the first-rank hadron. A simulation of the performance of the OPAL detector was used to account for the effects of resolution and geometrical acceptance [13].

4 Identification of Muons in Multihadronic Events

Muon candidates were identified by associating central detector tracks to track segments in the muon subdetectors. Track segments in the hadron calorimeter or muon chambers were straight lines of hits reconstructed independently in each subdetector. A hadron calorimeter track segment was formed if at least five layers had aligned clusters of strip hits consistent with the passage of a minimum ionizing particle. At least one of these clusters had to be in the outer four layers. In the muon detectors, with the exception of some restricted areas, a minimum of three hits was demanded for the reconstruction of a track segment. In the central detector, muon candidate tracks were required to be reconstructed from at least 40 hits in the jet chamber, and to have polar angles within the range $|\cos\theta| < 0.9$. Each central detector track was extrapolated through the surrounding material, allowing for energy loss, multiple scattering and measurement errors. On entering a muon subdetector, the position and direction of the extrapolated trajectory were compared with the position and direction of any muon track segment found in that particular subdetector. A track matching the position of both a hadron calorimeter and a muon chamber segment was classified as a muon. To maintain high efficiency, a track matching only one subdetector segment was also accepted if further conditions were satisfied. For muon candidates with a track segment in the muon chambers but not the hadron calorimeter, matching in direction was demanded as well as a better positional match. In addition, if the projected track passed through the hadron calorimeter, associated hits were required in at least half the layers. For candidates matched only to a hadron calorimeter segment, a better line-fit to the segment hits was demanded, with associated hits indicating penetration of at least 6 interaction lengths of iron. Where more than one central detector track matched a given muon segment, the track with the best matching likelihood was classified as a muon. When applied to Monte Carlo simulated events containing single prompt muon tracks, this procedure selected the wrong track as a muon in 1.3% of cases, for track momentum above 4.5 GeV/c.

The overall efficiency for the detection of muons in $Z^0 \to$ multihadrons was estimated from the muon finding efficiency in a sample of $e^+e^- \to \mu^+\mu^-$ events, selected using the central detector and electromagnetic calorimeter but not the hadron calorimeter or muon chambers. The residual contamination due to $\tau^+\tau^-$ hadronic decays was less than 0.5%. Small efficiency corrections (about 1%) were applied to account for the differences in isolation and momentum distribution between muons from $e^+e^- \to \mu^+\mu^-$ and muons in hadronic decays. These corrections, which dominate the uncertainty in the efficiency, were estimated by studying the difference in muon finding efficiency between simulated $e^+e^- \to \mu^+\mu^-$ events and simulated multihadronic events. Further checks on the efficiencies were also made using real data, by exploiting the inherent redundancy between the hadron calorimeter and the muon chambers. The fraction of muon candidates identified by one of these subdetectors and also found by the other was consistent with the expected efficiency and with Monte Carlo predictions. The overall efficiency was found to be $(85 \pm 2)\%$ in the range $|\cos\theta| < 0.8$. In the range $0.8 < |\cos\theta| < 0.9$,

a lower efficiency, $(77 \pm 4)\%$, was found, due to the combined effects of falling tracking efficiency and limited hadron calorimeter acceptance in this region. The efficiency is approximately independent of muon momentum and transverse momentum for $p > 4.5$ GeV/c.

Hadronic contamination in the muon candidates was determined by using a Monte Carlo simulation of multihadronic events. The observed fraction of muon candidates found by the various subdetectors as the muon selection criteria were varied was found to be well represented, giving confidence in the details of the detector simulation. The probability for a hadron to be misidentified as a muon was found to be weakly dependent upon momentum and transverse momentum with an average value of 1.3% per track for momenta above 4.5 GeV/c. The reliability of this Monte Carlo prediction was checked using kinematically identified $K^0_S \rightarrow \pi^+\pi^-$ decays in the OPAL data sample. Pions with momenta above 4.0 GeV/c were selected. Their mean momentum was 5.8 GeV/c. The fraction which were identified as muons was $(0.80 \pm 0.14)\%$ in data as compared with $(1.1 \pm 0.1)\%$ for Monte Carlo simulated events. A similar study of 3-prong τ decays, where the pions have momenta in the range 3 to 30 GeV/c, yielded a $(1.4 \pm 0.3)\%$ probability for misidentification of a pion as a muon, compared with $(1.2 \pm 0.1)\%$ predicted by the Monte Carlo. The statistical accuracy of these comparisons translates into an overall systematic uncertainty of about 15% in the background due to pions. However, pions account for only about half the total number of non-prompt muon candidates, the remainder being mostly due to kaons. The contribution from decays is about half the total for both kaons and pions. Whilst the differences between kaons and pions in both sail-through and punch-through probabilities are expected to be well described by the Monte Carlo, the kinematics of $K \rightarrow \mu\nu$ decays are different from $\pi \rightarrow \mu\nu$ decays. Since the kaon background has not been cross-checked, we have conservatively assigned an error of 50% to the $K \rightarrow \mu\nu$ decay contribution, which is approximately one quarter of the total background. Combining linearly the estimated errors on all the background contributions results in a systematic uncertainty of 25% in the overall misidentification probability.

5 Measurement of the Branching Ratios

We identified a total of 12,350 hadronic events containing a muon candidate track with momentum $p > 3.0$ GeV/c. For each event, the scaled mass jet finding algorithm of JADE [14], employing the E0 recombination scheme [15], was used to group charged tracks into jets. To ensure that jets were well contained within the active detector volume, the polar angle of the axis of the jet containing the muon was required to be in the range $|\cos\theta_{jet}| < 0.8$. The value of the jet resolution parameter y_{cut} was chosen to be 0.02. Thereby most of the decay products from a b flavoured hadron were included into a single jet, while good resolution of two and three jet events was maintained. Monte Carlo studies showed that the axis of the jet containing the muon candidate track (evaluated with the muon included) gave a good estimate of the direction of the parent hadron. The transverse momentum, p_T, of the muon candidate was calculated with respect to this axis.

In order to extract the b quark component of the observed signal, two different methods were employed. In the first method, the b fraction was determined by counting the number of muons with high p and p_T after subtracting estimated backgrounds. This kinematic region is expected to be dominated by the decays of b flavoured hadrons. The backgrounds to be subtracted were estimated using the Monte Carlo simulation. The second method used the predicted shape of the muon spectra from the processes (a) to (e), described in Section 1, to fit the observed distributions in p and p_T. This procedure enabled the fraction of events

due to b and c decays to be extracted, along with b and c quark fragmentation parameters. The two determinations of the $Z^0 \to b\bar{b}$ partial width are complementary, since they are subject to different systematic uncertainties. For the counting method, the uncertainty due to hadronic background subtraction dominates, whereas the systematic error in the fitting method depends on several factors such as the shape of the component spectra, the size of the cascade contribution and the details of fragmentation.

5.1 Counting Muons with Large p and p_T

In this method, the number of muons from b decays was determined using the kinematic region $p > 4.5$ GeV/c, $p_T > 1.0$ GeV/c where the contributions from charm and cascade reactions, as well as hadronic contamination, are suppressed. The distribution in p_T is shown in Fig.1a for the 8,692 muon candidates with momenta greater than 4.5 GeV/c. Fig.1b shows the momentum distribution of the muon candidates with $p_T > 1.0$ GeV/c. The Monte Carlo predicted distributions [8], assuming Standard Model values for the partial widths $Z^0 \to b\bar{b}$ and $Z^0 \to c\bar{c}$, are superimposed in each case. As previously mentioned, the normalisation of the hadronic contamination is subject to a 25% systematic uncertainty. For the charm quark fragmentation, we chose $\langle x_E \rangle_c = 0.55$, consistent with an average of PEP and PETRA experiments [16]. For the b quarks, we estimated $\langle x_E \rangle_b = 0.70 \pm 0.02$ by measuring the mean momentum of muon candidates in the b enriched region with $p_T > 1.5$ GeV/c. The relationship between this mean momentum and $\langle x_E \rangle_b$ was derived from a series of Monte Carlo simulations. The error is statistical only. The hadronic contamination component was obtained by applying the p and p_T dependent misidentification probability (found from Monte Carlo studies) to all tracks observed in the multihadron data which passed the track selection cuts (i.e. all potential fake muons). This technique reduced dependence on the precise simulation of event topology and track multiplicity.

The fraction of b quark events was determined using:

$$\frac{\Gamma(Z^0 \to b\bar{b})}{\Gamma(Z^0 \to \text{hadrons})} \times \text{Br}(b \to \mu) = \frac{N_\mu^{obs} - N_\mu^c - N_\mu^{fake}}{2 \times N_{Z^0} \times \eta \times (1 + f_{acc} f_{br})} \qquad (1)$$

where $N_\mu^{obs}, N_\mu^c, N_\mu^{fake}$ are the observed number of muons, the predicted number of muons from charm decays and the contribution of hadronic background, respectively. N_{Z^0} is the total number of $Z^0 \to$ hadrons events (133,310), and η is the product of the efficiency for muon identification (0.85 ± 0.02), the efficiency of the kinematic cuts (0.355 ± 0.005) and the geometrical acceptance including detector resolution (0.76 ± 0.01). The last term in the denominator accounts for the contribution of the cascade component, where $f_{br} = \text{Br}(b \to c \to \mu X)/\text{Br}(b \to \mu X)$ and f_{acc} is the ratio of the kinematic acceptance for muons from the cascade process to that for muons from direct b quark decays. We used $f_{acc} = 0.121 \pm 0.002$, estimated from Monte Carlo studies. The parameter f_{br} was derived from the results $\text{Br}(b \to c \to \mu X) = 0.102 \pm 0.010 \pm 0.007$ [17] and $\text{Br}(b \to \mu X) = 0.102 \pm 0.002 \pm 0.007$ [18], obtained from fits to the inclusive lepton spectrum at the $\Upsilon(4S)$. These yield the value $f_{br} = 1.0 \pm 0.1 \pm 0.1$. The systematic error on f_{br} has been increased to 20%, to allow for the uncertainty due to the mixture of b flavoured hadrons being different at LEP [19]. The charm contribution was estimated by using the prediction of the Standard Model for $\Gamma(Z^0 \to c\bar{c})/\Gamma(Z^0 \to \text{hadrons})$=0.171 [20] and $\text{Br}(c \to \mu) = (7.9 \pm 0.9)\%$, obtained from an average of PEP and PETRA measurements [11]. The contribution of $b \to \tau \to \mu$ was neglected, since it is expected to contribute < 2% of all $b \to \mu$ decays.

We found a total of 2269 events with muons in the kinematic region, $p > 4.5$ GeV/c and

$p_T > 1.0$ GeV/c. The predictions for the charm component and the hadronic contamination were 106 and 669, respectively.

Using (1), we found:

$$(\Gamma(Z^0 \to b\bar{b})/\Gamma(Z^0 \to \text{hadrons})) \times \text{Br}(b \to \mu) = 0.0218 \pm 0.0007 \pm 0.0026,$$

where the errors are statistical and systematic, respectively.

The systematic error is due to the uncertainties in the normalisation of the hadronic contamination, the predictions of the cascade and the charm components and the fragmentation parameters. The dominant source is the 25% uncertainty in the normalisation of the hadronic background. Varying both the cascade and charm components by 25% changed the result by less than 4%. The value of $\langle x_E \rangle_b$ was allowed to vary within one standard deviation of the measured value, resulting in a 2.4% change in the result. The estimated 3% uncertainty in the efficiency η is directly reflected in a 3% systematic error in the final result.

5.2 Fitting the p and p_T Distributions

In this method, the observed p *vs* p_T spectrum for muons was fitted by a combination of the p *vs* p_T distributions for each of the separate sources of prompt and non-prompt muons. The contribution from each source was allowed to vary, so that the sum of the contributions reproduced the observed distribution. This procedure determined the flavour composition of the inclusive muon sample, along with values for $\langle x_E \rangle_b$ and $\langle x_E \rangle_c$.

The shape of each of the components was predicted by the Monte Carlo simulation. The ratio f_{br}, described in Section 5.1, was used to constrain the ratio between the $b \to c \to \mu$ cascade component and the direct $b \to \mu$ component. For the b and c quarks, events were generated in bins of the respective b and c fragmentation variables (x_E or z, as defined below), and the shape of the p *vs* p_T spectrum was found for each bin separately. The relative proportion of b and c quark events from each bin was constrained to vary according to the form of the Peterson fragmentation function. The non-prompt backgrounds originating from (uds), c and b events all have slightly different shapes, which were determined separately using the same Monte Carlo. The muon misidentification probability per track was assumed to be the same for heavy quark events as for light quark events. In addition, the backgrounds from b and c quarks were constrained to be proportional to the fitted branching fractions $(\Gamma(Z^0 \to b\bar{b})/\Gamma(Z^0 \to \text{hadrons})) \times \text{Br}(b \to \mu)$ and $(\Gamma(Z^0 \to c\bar{c})/\Gamma(Z^0 \to \text{hadrons})) \times \text{Br}(c \to \mu)$. This allowed for uncertainties in the overall background normalisation, and for the differences between the measured Z^0 branching ratios and those used in the simulation of the background processes.

Ideally, the shape of the Monte Carlo predicted p *vs* p_T spectrum in a given bin of the fragmentation variable should not be sensitive to QCD model parameters or to the form of the fragmentation function. Such model dependence can be reduced by a suitable choice of the fragmentation variable and an appropriate definition of p_T.

In the Monte Carlo, the fragmentation function is parametrized in terms of the fraction, z, of available energy carried by the first-rank hadron. This fraction is not directly related to the fragmentation variable x_E, because of the influence of gluon radiation upon the maximum available energy. In simple terms, gluon emission tends to reduce this available energy, reducing the value of x_E, while simultaneously affecting the jet structure of the event. The fit results

using x_E as the fragmentation variable are sensitive to the accuracy of QCD modelling and to the chosen form of fragmentation function, whereas those using z should be much less sensitive [21].

The muon transverse momentum, p_T, was measured relative to a jet axis evaluated including the muon. Transverse momentum can also be measured with respect to the thrust axis of the event, or the jet axis re-evaluated with the muon excluded. Using the thrust axis introduces QCD dependence, because gluon radiation affects the angle between this axis and the direction of the primary hadron. Excluding the muon from the jet gives a p_T which on its own is a better flavour discriminator, but is a less accurate measure of the true p_T and is more strongly correlated with p. We have repeated the fit for all three definitions of p_T, using both x_E and an approximation to z [22].

The results of the binned maximum likelihood fit to the observed p *vs* p_T distributions under various conditions are shown in Table 1. (When z was used, the mean values obtained were converted into corresponding mean values of the physical variable x_E using the Monte Carlo simulation. This conversion is therefore model-dependent). A χ^2 test was applied to each fit to give some indication of comparative quality.

Our least model-dependent measurement is result A, obtained by fitting the whole p *vs* p_T spectrum for $p > 4.5$ GeV/c, using z as the fragmentation variable, and defining p_T with respect to the jet axis evaluated with the muon included. The fitted contributions according to this result are shown superimposed on the data in Fig.2a and Fig.2b. There is a strong (88%) anti-correlation between the $c\bar{c}$ and background contributions, producing a large statistical error in the charm product branching ratio and in $\langle x_E \rangle_c$. Repeating the fit with no $c\bar{c}$ component reduced the fitted $b\bar{b}$ fraction by 3.5%, while the χ^2 per degree of freedom worsened to 291/280. Results B and C correspond to repeating A with p_T defined with respect to different axes. The change in the $b\bar{b}$ fraction when p_T is re-defined with respect to the thrust axis is an indication of the maximum sensitivity to the modelling of processes such as hard gluon radiation which affect the p_T distribution. We expect these possible systematic effects to be minimised for result A.

As a further cross-check, for result D the fit was restricted to the kinematic region $p_T > 1.0$ GeV/c, $p > 4.5$ GeV/c and the charm parameters were fixed at the Standard Model values. The product branching ratio and $\langle x_E \rangle_b$ values obtained agreed with the counting result, although the correlation obtained from the fit between the b quark and background distributions was 89%, as compared with 40% when the whole p_T range was considered. The fitted fraction of hadronic background events, (26 ± 4)%, agreed with the estimate in Section 5.1 (29 ± 7)%, and the shape of the fitted background distribution in p and p_T agreed with that derived using observed tracks, as described in Section 5.1.

Results E,F,G,H correspond to modelling fragmentation in terms of the variable x_E, again choosing three different axes for the definition of p_T. The insensitivity of the result to the change in fragmentation variable provides evidence that, for our choice of p_T, errors due to inadequate QCD modelling are small.

The estimated systematic errors from various sources are listed as items (1) to (6) in Table 2. Error (1) accounts for possible inadequacies in the Monte Carlo representation of the p and p_T resolution. The error was estimated from the change in results produced by varying the track polar angle resolution by ± 25 mrad for 10% of simulated tracks. This variation produced significant deviations between the observed and simulated p_T spectra. The additional uncertainty in the shape of the background distribution (2) was investigated by changing the

punch-through contribution by ±25%, which caused a change of about ±10% in the slope of the overall background as a function of momentum. We also accounted for the uncertainty in the muon detection efficiency (3), and in the number of $b \to c \to \mu$ cascade decays (4). The error (4) was assigned by studying the change produced when the parameter f_{br} (see Section 5.1) was varied by 20%. The uncertainty introduced by limited Monte Carlo statistics and the systematic effects of varying the binning used for the fit were included in (5). The fitted $b\bar{b}$ fraction was stable when details of the fitting procedure were changed, whereas the $c\bar{c}$ fraction fluctuated because of the high anti-correlation between the c quark and background contributions. Finally the changes produced by assuming different forms for the fragmentation function [23] were used to derive the last contribution (6). The influence of the kinematic cuts upon the result was found to be small. The fitted $b\bar{b}$ fraction changed by less than 5% when the momentum cut was varied between 4.0 GeV/c and 6.0 GeV/c, or when a p_T cut of 0.5 GeV/c was applied. We have not considered the effect on the results of uncertainties in the modelling of semi-leptonic b and c quark decays. Taking the systematic effects (1) to (6) into account gave the result:

$$\frac{\Gamma(Z^0 \to b\bar{b})}{\Gamma(Z^0 \to \text{hadrons})} \times \text{Br}(b \to \mu) = 0.0226 \pm 0.0007 \pm 0.0013$$

$$\frac{\Gamma(Z^0 \to c\bar{c})}{\Gamma(Z^0 \to \text{hadrons})} \times \text{Br}(c \to \mu) = 0.0176 \pm 0.0025 \pm 0.0042$$

$$\langle x_E \rangle_b = 0.726 \pm 0.007 \pm 0.022$$

$$\langle x_E \rangle_c = 0.56 \pm 0.02 \pm 0.03$$

5.3 Extraction of the Partial Widths

The average semi-leptonic branching ratio $\langle \text{Br}(b \to \mu X) \rangle$, measured at lower energies, can be used to extract the value of $\Gamma(Z^0 \to b\bar{b})/\Gamma(Z^0 \to \text{hadrons})$. However, as previously mentioned, the average semi-leptonic branching ratio may be different at LEP if b flavoured hadrons have different lifetimes and are produced with different relative abundances compared with lower energies [19].

Using the measurements from the e^+e^- continuum [11] $\text{Br}(b \to \mu X) = 0.117 \pm 0.013$, and $\text{Br}(c \to \mu X) = 0.079 \pm 0.009$, combined with the results from Section 5.2, gave:

$$\Gamma(Z^0 \to b\bar{b})/\Gamma(Z^0 \to \text{hadrons}) = 0.193 \pm 0.006(\text{stat}) \pm 0.011(\text{syst}) \pm 0.021(\text{br.ratio}),$$

$$\Gamma(Z^0 \to c\bar{c})/\Gamma(Z^0 \to \text{hadrons}) = 0.223 \pm 0.032(\text{stat}) \pm 0.053(\text{syst}) \pm 0.025(\text{br.ratio}).$$

These results are consistent with the Standard Model predictions [20]: $\Gamma(Z^0 \to b\bar{b})/\Gamma(Z^0 \to \text{hadrons}) = 0.217$, and $\Gamma(Z^0 \to c\bar{c})/\Gamma(Z^0 \to \text{hadrons}) = 0.171$. The partial widths and the accompanying fragmentation parameter values are in good agreement with measurements made by other experiments [4].

Using $\text{Br}(b \to \mu X) = 0.117 \pm 0.013$, combined with a measurement by OPAL of the hadronic width [24], $\Gamma(Z^0 \to \text{hadrons}) = 1739 \pm 17$ MeV, gave the result:

$$\Gamma(Z^0 \to b\bar{b}) = 336 \pm 10(\text{stat}) \pm 20(\text{syst}) \pm 37(\text{br.ratio}) \text{ MeV}.$$

where the uncertainty in the hadronic width was included in the systematic error.

6 Measurement of the Forward-Backward Asymmetry

The angular distribution for $e^+e^- \to Z^0 \to b\bar{b}$ is:

$$d\sigma/d\cos\theta \propto (1 + \cos^2\theta + \frac{8}{3} A_b^{FB} \cos\theta), \tag{2}$$

where θ is the angle between the b quark momentum and the outgoing electron beam. The forward-backward asymmetry, A_b^{FB}, can be measured using:

$$A_b^{FB} = \frac{\sigma_F - \sigma_B}{\sigma_F + \sigma_B}, \tag{3}$$

where σ_F and σ_B are the b quark cross sections in the forward and backward hemispheres, respectively. σ_F and σ_B can be expressed in terms of the number of observed decays of b flavoured hadrons in each hemisphere, N_F and N_B. Since A_b^{FB} is strongly dependent on the centre of mass energy, we restricted this analysis to the hadronic data sample collected near the Z^0 peak, corresponding to 105,589 events with centre of mass energies between 91.0 and 92.0 GeV. The off-peak data sample is still too small to yield a statistically worthwhile measurement.

The direction of the thrust axis of the event, calculated using charged tracks, was used to estimate the angle θ. Monte Carlo studies showed that this axis best represented the direction of the primary b quark at production. (The muon transverse momentum was defined relative to the jet axis calculated with the muon included in the jet.) The thrust axis was required to lie within the angular range $|\cos\theta| < 0.9$. No restriction was placed on the polar angle of the jet axis. Tracks used in calculating both jet and thrust axes were required to be reconstructed from at least 20 hits in the jet chamber (corresponding to an approximate angular range $|\cos\theta| < 0.95$). However, for muon candidate tracks, the more stringent requirement of 40 hits and $|\cos\theta| < 0.9$ was retained. The charge of the b quark was tagged using the charge of the muon candidate, Q_μ. The probability of misidentifying the charge of a muon candidate of momentum less than 30 GeV/c with $|\cos\theta| < 0.9$ was estimated to be $< 0.5\%$ using the observed charge confusion in $e^+e^- \to \mu^+\mu^-$ events. Fig.3 shows the distribution in $-Q_\mu \cos\theta$ for events with muon candidates in the kinematic region $p > 4.5$ GeV/c and $p_T > 1.0$ GeV/c, after subtraction of the $c\bar{c}$ and hadronic background contributions and correction for the muon identification efficiency. The errors due to efficiency and hadronic background subtraction are correlated between the forward and backward regions. The $c\bar{c}$ contribution was calculated using the Standard Model expectation as described in Section 5.1. The hadronic background was calculated by weighting the observed $\cos\theta$ distribution of all tracks by the $|\cos\theta|$ dependent muon misidentification probability per track. The $|\cos\theta|$ dependent efficiency correction took into account the acceptance effects caused by restricting the thrust axis and the muon direction to a fiducial volume $|\cos\theta| < 0.9$. The overall efficiency in the extreme bins of $\cos\theta$ was estimated to be $(60 \pm 6)\%$.

After subtracting backgrounds, applying all corrections and extrapolating to the full $\cos\theta$ range, we used (3) to determine:

$$A^{FB}(\text{Observed}) = 0.049 \pm 0.036,$$

where the errors are statistical only. Fitting the angular distribution to (2) using a χ^2 method, accounting for the correlations between the errors in different bins, yielded:

$$A^{FB}(\text{Observed}) = 0.058 \pm 0.034,$$

corresponding to the curve shown in Fig. 3. The χ^2 is 4 for 10 degrees of freedom.

The observed asymmetry was then corrected for the effects of the cascade decays $b \to c \to \mu^+$ (which has an equal but opposite asymmetry to the direct $b \to \mu^-$ process) and $b \to cW^-$, with $W^- \to s\bar{c}$ and $\bar{c} \to \mu^-$ (which has the same asymmetry as the direct process). The overall impact is to reduce the observed asymmetry to 81% of the underlying $b\bar{b}$ asymmetry. After allowing for this, we obtained:

$$A_b^{FB} = 0.060 \pm 0.044 \pm 0.010, \text{ from counting, and}$$
$$A_b^{FB} = 0.072 \pm 0.042 \pm 0.010, \text{ from fitting.}$$

In both cases the assigned systematic uncertainty of ± 0.010 is composed of contributions from the subtracted hadronic background (± 0.007), the subtracted $c\bar{c}$ component and the cascade correction (± 0.006), and the possible effects of track mismatching and charge misidentification (± 0.002). Neither the counting nor the fitting result was significantly affected when the overall correction to the outer bins was varied by $\pm 10\%$.

In order to compare with Standard Model predictions, the value of A_b^{FB} was corrected for the effect of $B^0\bar{B}^0$ mixing, which reduces the true asymmetry by a factor of (1-2χ), where χ is the average mixing rate defined as,

$$\chi = (B \to \bar{B} \to \mu^-)/((B \to \bar{B} \to \mu^-) + (B \to B \to \mu^+)).$$

Various measurements of χ have been reported [25], for B_d^0 and for mixtures of b flavoured hadron species. We assumed the average mixing rate for b flavoured hadrons to be $\chi = 0.130$, consistent with these measurements and with the expected production ratio of the different species [19], if B_s mesons are assumed to have $\chi = 0.5$. Using this value of χ to correct the fitted asymmetry gave:

$$A_b^{FB}(\text{Corrected}) = 0.097 \pm 0.057 \pm 0.014,$$

consistent with the Standard Model prediction at the Z^0 peak, $A_b^{FB} = 0.09$ [20], and with other measurements [5]. The systematic error does not include any contribution from uncertainty in the mixing parameter.

In the Standard Model, the forward backward asymmetry for $Z^0 \to b\bar{b}$ at $s = M_Z^2$, without photonic corrections, can be written as:

$$A_b^{FB} = \frac{3\hat{v}_e\hat{a}_e\hat{v}_b\hat{a}_b}{(\hat{v}_e^2 + \hat{a}_e^2)(\hat{v}_b^2 + \hat{a}_b^2)},$$

where $\hat{v}_e$, $\hat{v}_b$, $\hat{a}_e$, $\hat{a}_b$ are the effective vector and axial vector couplings of the electron and b quark, respectively, in the improved Born approximation[2].

We used the relations $\hat{a}^2 = \rho_Z$ and $\hat{v}^2 = \rho_Z(1 + 4Q_f \sin^2\bar{\theta}_W)^2$, (where Q_f is the fermion charge) to obtain the effective weak mixing angle, $\sin^2\bar{\theta}_W$. Since A_b^{FB} depends only weakly on ρ_Z, we took ρ_Z from the Standard Model.

Using our measured value of A_{FB}, we obtained:

$$\sin^2\bar{\theta}_W = 0.232 \pm 0.010(\text{stat}) \pm 0.002(\text{syst}),$$

where QED and QCD corrections have been included. We have ignored the difference between $\sin^2\bar{\theta}_W$ for electrons and b quarks resulting from the presence of additional top quark diagrams, since this is expected [20] to be of order 0.0009.

7 Summary

We have analysed 8,692 muon candidates in approximately 133,000 hadronic decays of the Z^0 boson. By fitting the p *vs* p_T distribution, using Monte Carlo simulations of the shape of the spectra expected from background and from the decays of b and c flavoured hadrons, we obtained:

$$(\Gamma(Z^0 \to b\bar{b})/\Gamma(Z^0 \to \text{hadrons})) \times \text{Br}(b \to \mu) = 0.0226 \pm 0.0007(\text{stat}) \pm 0.0013(\text{syst}).$$

The fit also yielded:

$$(\Gamma(Z^0 \to c\bar{c})/\Gamma(Z^0 \to \text{hadrons})) \times \text{Br}(c \to \mu) = 0.0176 \pm 0.0025(\text{stat}) \pm 0.0042(\text{syst}),$$

$$\langle x_E \rangle_b = 0.726 \pm 0.007(\text{stat}) \pm 0.022(\text{syst}),$$

$$\langle x_E \rangle_c = 0.56 \pm 0.02(\text{stat}) \pm 0.03(\text{syst}).$$

A complementary analysis of the $b\bar{b}$ fraction, based on counting the number of muons with $p_T > 1.0$ GeV/c and $p > 4.5$ GeV/c, and subtracting the contributions from background and c quark decays, gave:

$$(\Gamma(Z^0 \to b\bar{b})/\Gamma(Z^0 \to \text{hadrons})) \times \text{Br}(b \to \mu) = 0.0218 \pm 0.0007(\text{stat}) \pm 0.0026(\text{syst}),$$

which supports the fitting result and is subject to different systematic uncertainties.

Using events with high p_T muons, the forward-backward asymmetry of the reaction $e^+e^- \to Z^0 \to b\bar{b}$ at the Z^0 peak, before correction for $B^0\bar{B}^0$ mixing, was measured to be:

$$A_b^{FB} = 0.072 \pm 0.042(\text{stat}) \pm 0.010(\text{syst}).$$

Acknowledgements:

It is a pleasure to thank the SL Division for their efficient operation of the LEP machine and their continuing close cooperation with our experimental group. In addition to the support staff at our institutions we are pleased to acknowledge the following: The Bundesministerium fur Forschung und Technologie, FRG; The Department of Energy, USA; The Institute de Recherche Fondamentale du Commissariat a l'Energie Atomique; The Israeli Ministry of Science; The Minerva Gesellschaft; The National Science Foundation, USA; The Natural Sciences and Engineering Research Council, Canada; The Japanese Ministry of Education, Science and Culture (the Monbusho) and a grant under Monbusho International Science Research Program; The American Israeli Bi-national Science Foundation; The Science and Engineering Research Council, UK and The A. P. Sloan Foundation.

References

[1] MARK II Collaboration, G.S. Abrams et al., Phys. Rev. Lett. 63 (1989) 2173, and Phys. Rev. Lett. 63 (1989) 2780;
OPAL Collaboration, M.Z. Akrawy et al., Phys. Lett. B240 (1990) 497, and Phys. Lett. B247 (1990) 458;
ALEPH Collaboration, D. Decamp et al., Phys. Lett. B235 (1990) 339, and Z. Phys C48 (1990) 365;
L3 Collaboration, B. Adeva et al., Phys. Lett. B236 (1990) 109, Phys. Lett. B237 (1990) 136, and Phys. Lett. B238 (1990) 122;
DELPHI Collaboration, P. Aarnio et al., Phys. Lett. B241 (1990) 425, and P. Abreu et al., Phys. Lett. B241 (1990) 435.

[2] M. Consoli and W. Hollik, in Z physics at LEP1 ed. G. Altarelli et al., CERN 89-08, Vol. 1 (1989) 7.

[3] J. H. Kühn and P. M. Zerwas, in Z physics at LEP1 ed. G. Altarelli et al., CERN 89-08, Vol. 1 (1989) 267.

[4] MARK II Collaboration, J. F. Kral et al., Phys. Rev. Lett. 64 (1990) 1211.
L3 Collaboration, B. Adeva et al., Phys. Lett. B241, (1990) 416, and L3 Preprint #27 February 1991.
ALEPH Collaboration, D. Decamp et al., Phys. Lett 244B (1990) 555.
DELPHI Collaboration, P. Abreu et al., CERN-PPE/90-118.

[5] L3 Collaboration, B. Adeva et al., Phys. Lett. B 252 (1990) 713.

[6] K. Ahmet et al, The OPAL detector at LEP, CERN-PPE/90-114 to be published in Nucl. Instr. and Meth.

[7] OPAL Collaboration, M. Z. Akrawy et al., Phys. Lett. B231 (1989) 530, and Phys. Lett. B235 (1990) 389.

[8] T. Sjöstrand et al., Comp. Phys. Comm. 39 (1986) 347; and Comp. Phys. Comm. 43 (1987) 367.

[9] OPAL Collaboration, M. Z. Akrawy et al., Z. Phys. C47 (1990) 505.

[10] C. Quigg and J. L. Rosner, Phys. Rev. D19 (1979) 1532.

[11] J.J. Hernandez et al., Particle Data Book: Phys. Lett. 239B(1990) 1.

[12] C. Peterson et al., Phys. Rev. D27 (1983) 105.

[13] J. Allison et al., Comp. Phys. Comm. 47 (1987) 55;
R. Brun et al., GEANT 3, CERN Report DD/EE/84-1 (1989).

[14] W. Bartel et al., Z. Phys. C33 (1986) 23 and
S. Bethke et al., Phys. Lett. B213 (1988) 235.

[15] OPAL Collaboration, M. Z. Akrawy et al., CERN-PPE/90-143,
submitted to Z. Phys. C.

[16] A compilation of fragmentation results is given in:
JADE collaboration, W. Bartel et al., Z.Phys. C33 (1987) 339
Extrapolation to the Z^0 pole suggests a lower value $\langle x_E \rangle_c \simeq 0.50$, see for instance:
T. Sjöstrand et al., in Z Physics at LEP1, ed. G. Altarelli et al.,
CERN 89-08, Vol.3 (1989) 310.

[17] CLEO collaboration, reported by J. Alexander in *Les Rencontres de Physique de la Vallée d'Aosta*, La Thuile, Aosta Valley, Italy, (1990), to be published in Phys. Rev. D.

[18] CLEO collaboration, R.Fulton et al., Phys.Rev.Lett. 64, 16(1990).

[19] Assuming relative production rates during fragmentation for $u\bar{u}$:$d\bar{d}$:$s\bar{s}$:diquarks of 1.0:1.0:0.3:0.1 gives production ratios of 41%B_d, 41%B_u, 12.5%B_s and 5.5%B_{baryon}, consistent with the measured yield of hadrons of various flavours in e^+e^- annihilation at lower energies.
For reviews see:
T. Sjöstrand et al., in Z physics at LEP 1, ed. G.Altarelli et al.,
CERN 89-08, Vol 3 (1989) 143;
D.H. Saxon, "Quark and Gluon Fragmentation", in High Energy Electron Positron Annihilations, ed. A. Ali and P. Söding, pub. World Scientific;
D. Bortoletto et al., Phys Rev. D37, 1719 (1988).
Allowing the semi-leptonic branching ratios of B_s and B_{baryon} to differ from B_d and B_u by a factor 2, the average semi-leptonic branching ratio at LEP might be up to 20% different from that measured at the $\Upsilon(4S)$.

[20] Line shape program ZFITTER, Dubna-Zeuthen radiative correction group, (based on the ZBIZON package)
D. Yu. Bardin et al., Berlin-Zeuthen preprint PHE 89-19,1989.
R. Kleiss et al., in Z Physics at LEP1, CERN 89-08, ed. G. Altarelli et al.,
Vol. 3 (1989) 60.
(for the predictions used in this paper, the Z^0, top quark and Higgs boson masses were taken to be: $M_Z = 91.17\text{GeV}/c^2$, $M_{top} = 130\ \text{GeV}/c^2$, $M_{Higgs} = 100\ \text{GeV}/c^2$).

[21] J. Chrin, Manchester Preprint MAN/HEP/90-02 (1990).

[22] Since z was not accessible for the Monte Carlo data sample, we used the variable:

$$z_\theta = E_{hadron}/E_\theta, \text{ where } E_\theta = E_{quark} + \sum_i \frac{1}{(1+\theta_{qg_i})} E_{g_i} \ (\theta_{qg_i} < \theta_{max}),$$

which is shown in the above reference [21] to be a good approximation to z. Here θ_{qg_i} is the angle between the primary quark and the neighbouring gluon in the parton shower, g_i, which has energy E_{g_i}. The cut-off angle, θ_{max}, was set to 0.3 radians.

[23] B. Anderson, G. Gustafson and B. Söderberg, Z. Phys. C20 (1983) 317;
P. D. B. Collins and T. P. Spiller, J. Phys. G 11 (1985) 1289;
V. G. Kartvelishvili et al., Phys. Lett. 78B (1978) 615,
and Sov. J. Nucl. Phys. 38 (1985) 952.

[24] OPAL Collaboration, contributions to *Les Rencontres de Physique de la Vallée d'Aoste*, La Thuile, Aosta Valley, Italy (1991).

[25] For example:
UA1 Collaboration, C. Albajar et al., Phys. Lett. B 186 (1987) 27;
Phys. Lett. B 197 (1987) 565.
ARGUS collaboration, H.Albrecht et al., Phys. Lett. 192B, (1987) 245
CLEO collaboration, M.Artuso et al., Phys. Rev. Lett. 62 (1989) 2233
L3 Collaboration, B. Adeva et al., Phys. Lett. B 252 (1990) 703.
ALEPH Collaboration, D. Decamp et al., CERN-PPE 90-194,
submitted to Phys. Lett. B.

Figure Captions

Figure 1 p_T and p distributions for inclusive muon candidates showing Monte Carlo predictions for the various contributions.
a) p_T distribution for $p > 4.5$ GeV/c.
b) p distribution for $p > 4.5$ GeV/c and $p_T > 1.0$ GeV/c.
(The process $b \to \tau \to \mu$ is not included)
Note that p_T was defined with respect to the jet axis evaluated with the muon included.

Figure 2 Results of fitting for the composition of the observed p *vs* p_T distribution for $p > 4.5$ GeV/c and for all p_T, shown superimposed on:
a) the p_T distribution for $p > 4.5$ GeV/c.
b) the p distribution for $p > 4.5$ GeV/c and for all p_T.
(The process $b \to \tau \to \mu$ is included in the cascade contribution.)

Figure 3 Distribution of $-Q_\mu \cos\theta$ for the inclusive muon candidates, after background and efficiency corrections. The solid curve was obtained from a fit of the form:
$C \times (1 + \cos^2\theta + 8/3 A_b^{FB} \cos\theta)$.

Table 1

Fit	z	p_T *w.r.t.*	$\Gamma_{bb}/\Gamma_h \times \mathrm{Br}(b \to \mu)$	$\Gamma_{cc}/\Gamma_h \times \mathrm{Br}(c \to \mu)$	$\langle x_E \rangle_b$	$\langle x_E \rangle_c$	background	χ^2/dof
A	z_θ	jet (inc. μ)	0.0226 ± 0.0007	0.0176 ± 0.0025	0.726 ± 0.007	0.56 ± 0.02	$(43 \pm 5)\%$	259/282
B	z_θ	jet (exc. μ)	0.0239 ± 0.0007	0.0164 ± 0.0023	0.726 ± 0.008	0.55 ± 0.02	$(42 \pm 5)\%$	278/282
C	z_θ	thrust	0.0247 ± 0.0008	0.0153 ± 0.0023	0.717 ± 0.008	0.53 ± 0.02	$(42 \pm 4)\%$	308/282
D	z_θ	jet(inc. μ) $p_T > 1.0$ GeV/c	0.0224 ± 0.0013	0.0135 (fixed)	0.720 ± 0.009	0.55 (fixed)	$(26 \pm 4)\%$	140/158
E	x_E	jet (inc. μ)	0.0222 ± 0.0007	0.0163 ± 0.0030	0.74 ± 0.01	0.59 ± 0.04	$(43 \pm 6)\%$	263/282
F	x_E	jet(exc. μ)	0.0238 ± 0.0006	0.0150 ± 0.0019	0.72 ± 0.01	0.59 ± 0.04	$(42 \pm 4)\%$	270/282
G	x_E	thrust	0.0240 ± 0.0007	0.0159 ± 0.0020	0.73 ± 0.01	0.54 ± 0.04	$(42 \pm 4)\%$	271/282
H	x_E	jet(inc. μ) $p_T > 1.0$ GeV/c	0.0216 ± 0.0013	0.0135 (fixed)	0.74 ± 0.02	0.55 (fixed)	$(28 \pm 4)\%$	140/158

Table 1: Results of fits (using different fragmentation variables) to the sample of hadronic Z^0 decays containing muons with momentum above 4.5 GeV/c. The errors quoted are statistical only.

Table 2

Systematic	$\Gamma_{b\bar{b}}/\Gamma_h \times \mathrm{Br}(b \to \mu)$	$\Gamma_{c\bar{c}}/\Gamma_h \times \mathrm{Br}(c \to \mu)$	$\langle x_E \rangle_b$	$\langle x_E \rangle_c$
1) det. resolution	± 0.0007	± 0.0008	± 0.003	± 0.01
2) background shape	± 0.0003	± 0.0012	± 0.001	± 0.00
3) μ det. effic.	± 0.0005	± 0.0003	± 0.000	± 0.00
4) cascade contrib.	± 0.0006	± 0.0011	± 0.001	± 0.01
5) details of fit	± 0.0003	± 0.0037	± 0.011	± 0.02
6) frag. function	± 0.0006	± 0.0008	± 0.019	± 0.02
Total	± 0.0013	± 0.0042	± 0.022	± 0.03

Table 1: Systematic effects on the experimental measurements from the fitting method

Figure 1a

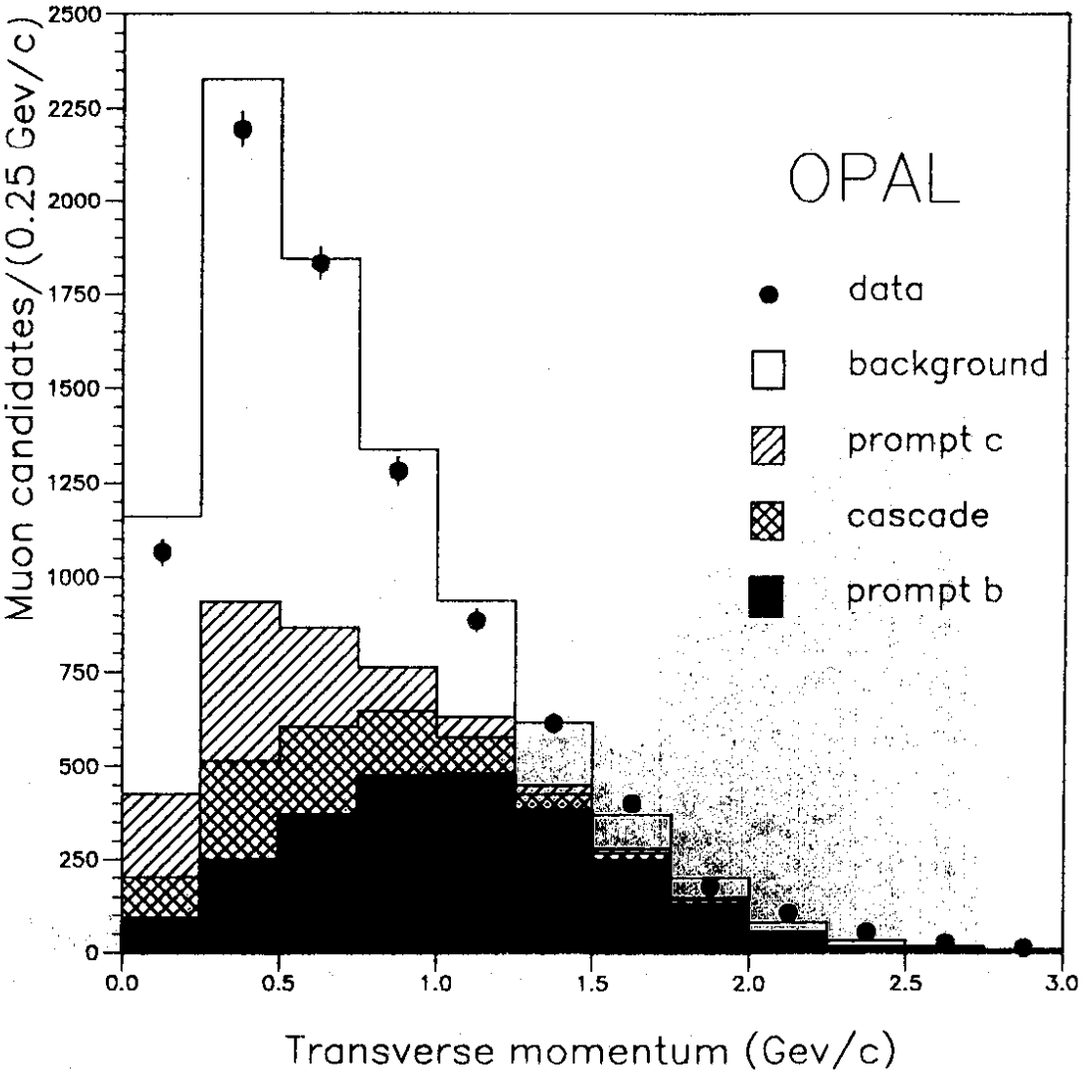
OPAL
data
background
prompt c
cascade
prompt b
Muon candidates/(0.25 Gev/c)
Transverse momentum (Gev/c)
2500
2250
2000
1750
1500
1250
1000
750
500
250
0
0.0
0.5
1.0
1.5
2.0
2.5
3.0

Figure 1b

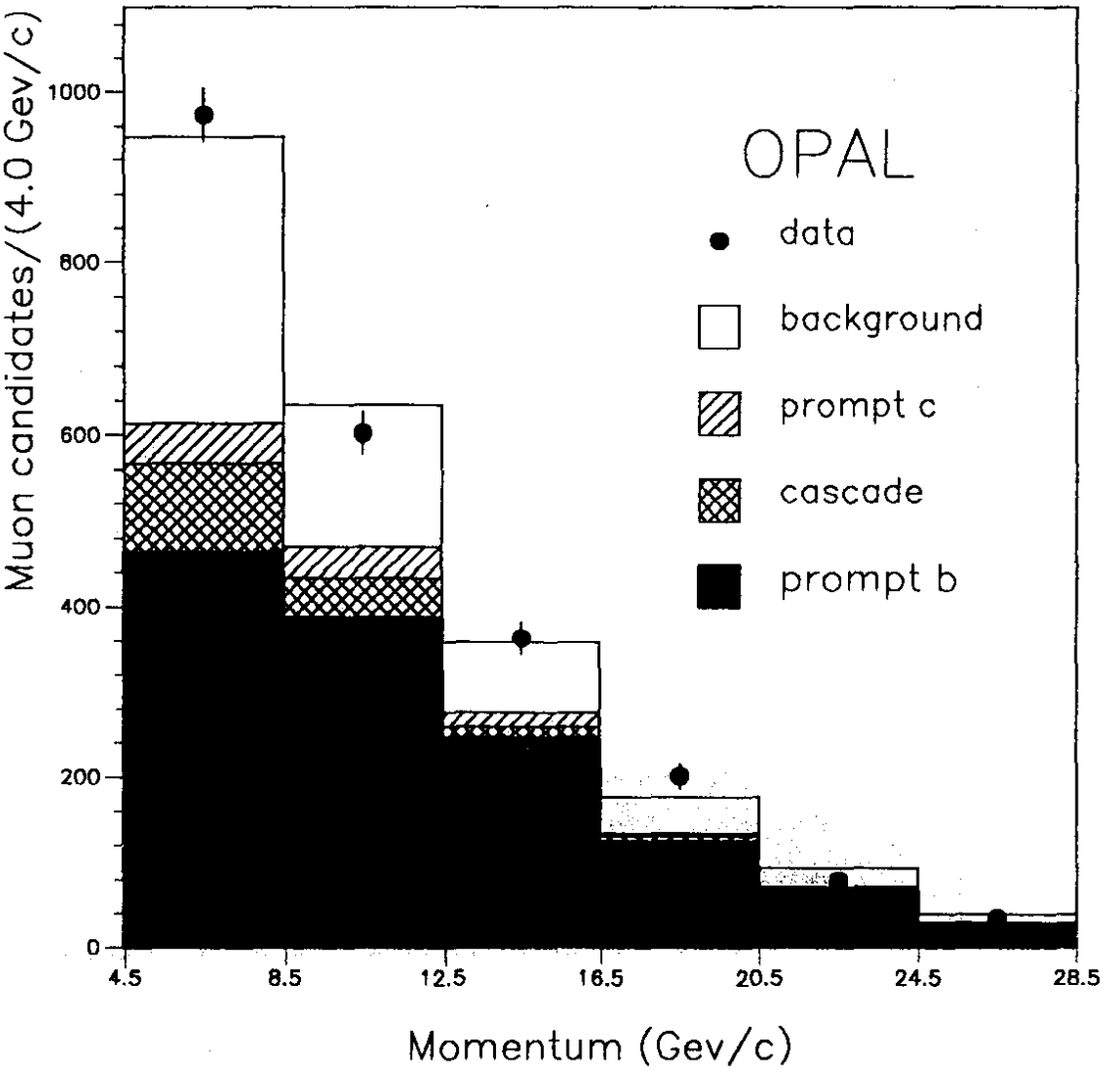
Muon candidates/(4.0 Gev/c)
1000
800
600
400
200
0
4.5
8.5
12.5
16.5
20.5
24.5
28.5
Momentum (Gev/c)
OPAL
data
background
prompt c
cascade
prompt b

Figure 2a

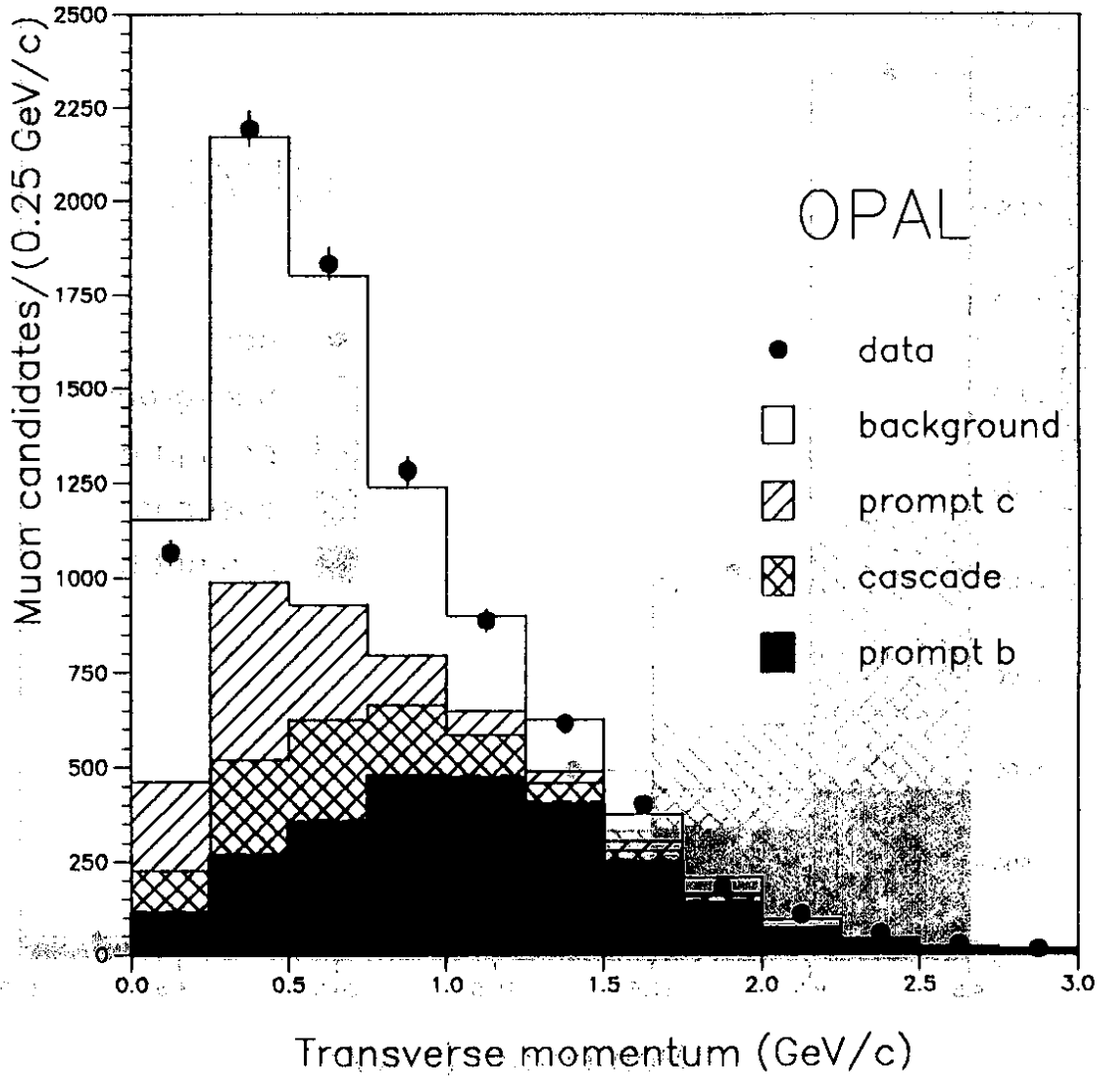
OPAL
data
background
prompt c
cascade
prompt b
Muon candidates/(0.25 GeV/c)
Transverse momentum (GeV/c)
2500
2250
2000
1750
1500
1250
1000
750
500
250
0
0.0
0.5
1.0
1.5
2.0
2.5
3.0

Figure 2b

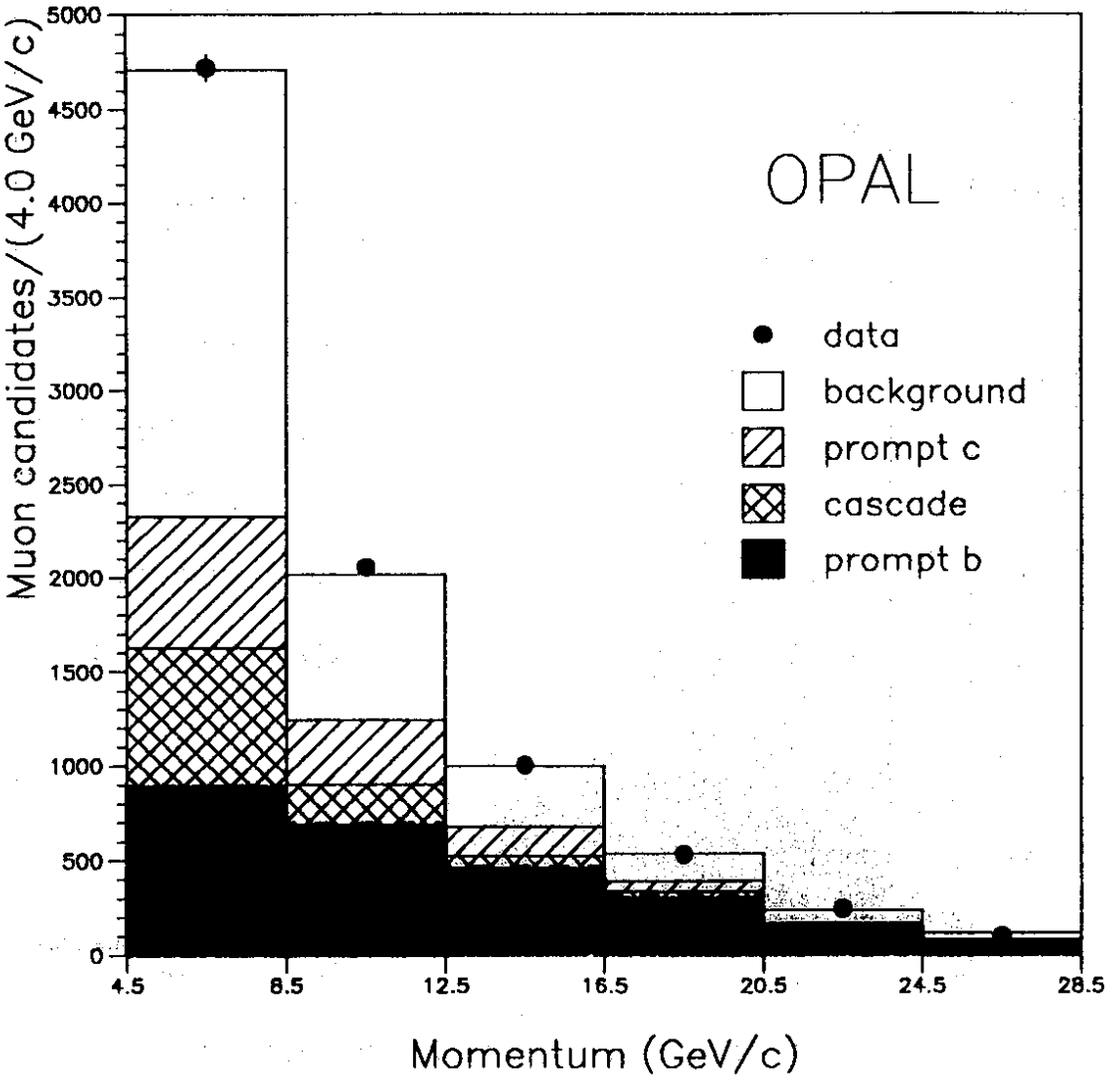
OPAL
data
background
prompt c
cascade
prompt b
Muon candidates/(4.0 GeV/c)
Momentum (GeV/c)
0
500
1000
1500
2000
2500
3000
3500
4000
4500
5000
4.5
8.5
12.5
16.5
20.5
24.5
28.5

Figure 3

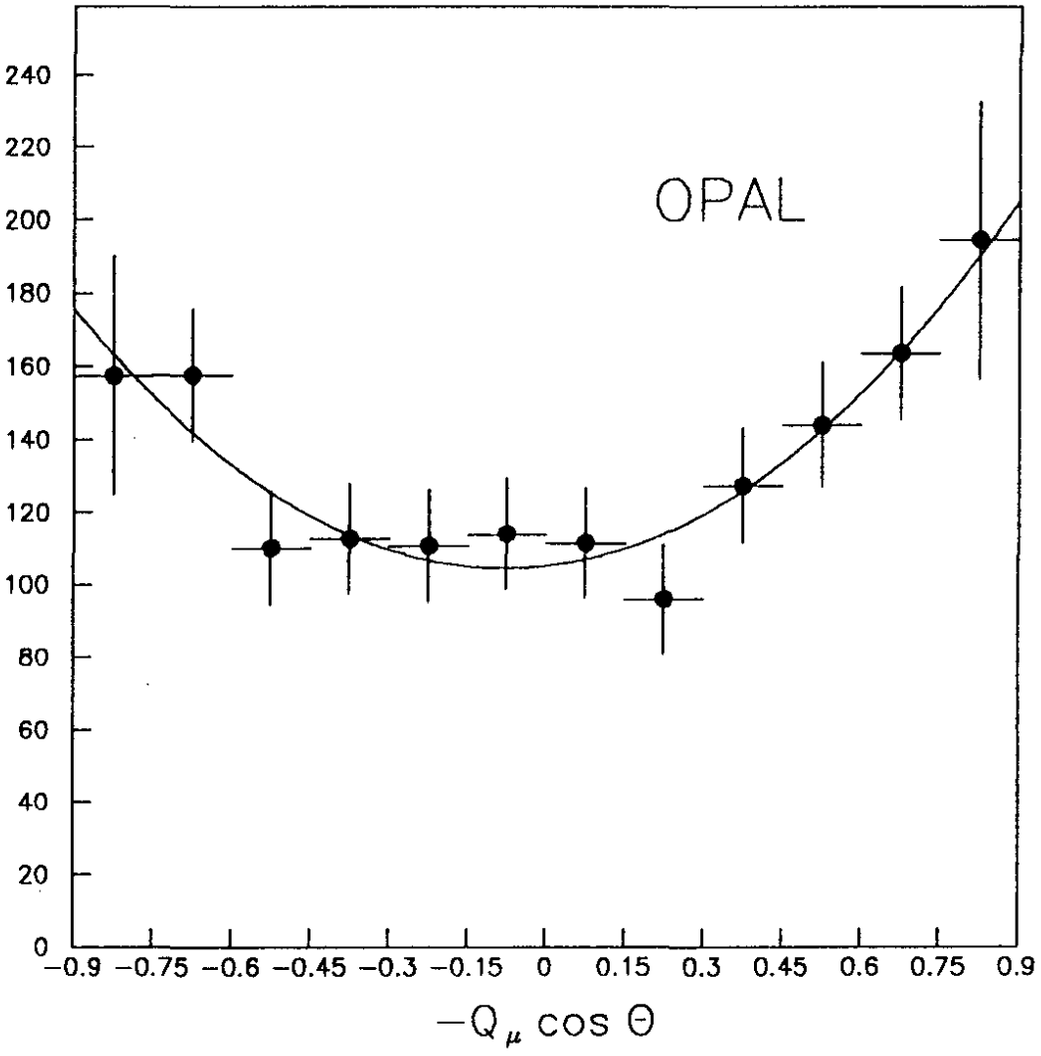

Imprimé au CERN. Prix : 0.85 Fr.